Regular Article

blood

RED CELLS, IRON, AND ERYTHROPOIESIS

Adenosine monophosphate deaminase 3 activation shortens erythrocyte half-life and provides malaria resistance in mice

Elinor Hortle,[1] Brunda Nijagal,[2] Denis C. Bauer,[3] Lora M. Jensen,[1] Seong Beom Ahn,[4] Ian A. Cockburn,[1] Shelley Lampkin,[1] Dedreia Tull,[2] Malcolm J. McConville,[5] Brendan J. McMorran,[1] Simon J. Foote,[1] and Gaetan Burgio[1]

[1]Department of Immunology and Infectious Disease, John Curtin School of Medical Research, Australian National University, Canberra, ACT, Australia; [2]Metabolomics Australia, Bio21 Institute, University of Melbourne, Parkville, VIC, Australia; [3]Commonwealth Scientific and Industrial Research Organization, Sydney, NSW, Australia; [4]Department of Biomedical Sciences, Faculty of Medicine and Health Sciences, Macquarie University, Sydney, NSW, Australia; and [5]Department of Biochemistry and Molecular Biology, Bio21 Molecular Science and Biotechnology Institute, University of Melbourne, Parkville, VIC, Australia

Key Points

- AMPD3 activation reduces red blood cell half-life, which is associated with increased oxidative stress and phosphatidylserine exposure.
- AMPD3 activation causes malaria resistance through increased RBC turnover and increased RBC production.

The factors that determine red blood cell (RBC) lifespan and the rate of RBC aging have not been fully elucidated. In several genetic conditions, including sickle cell disease, thalassemia, and G6PD deficiency, erythrocyte lifespan is significantly shortened. Many of these diseases are also associated with protection from severe malaria, suggesting a role for accelerated RBC senescence and clearance in malaria resistance. Here, we report a novel, *N*-ethyl-*N*-nitrosourea–induced mutation that causes a gain of function in adenosine 5′-monophosphate deaminase (AMPD3). Mice carrying the mutation exhibit rapid RBC turnover, with increased erythropoiesis, dramatically shortened RBC lifespan, and signs of increased RBC senescence/eryptosis, suggesting a key role for AMPD3 in determining RBC half-life. Mice were also found to be resistant to infection with the rodent malaria *Plasmodium chabaudi*. We propose that resistance to *P. chabaudi* is mediated by increased RBC turnover and higher rates of erythropoiesis during infection. (*Blood*. 2016; 128(9):1290-1301)

Introduction

The lifespan of red blood cells (RBC) is tightly regulated, lasting some 120 days in humans and 51 days in mice.[1] Senescent RBCs are cleared from the bloodstream by macrophages of the reticuloendothelial system and are replaced with new erythrocytes.[2-4] This destruction is not random, and it is highly dependent on RBC age.[4] The factors determining the rate of RBC aging, and thereby RBC lifespan, have not been fully elucidated.

In several genetic conditions, including pyruvate kinase deficiency, sickle cell disease, thalassemia, hereditary spherocytosis, and G6PD deficiency,[5,6] erythrocyte lifespan is significantly shortened. In most cases, cells show signs of increased senescence, including increased oxidative stress and phosphatidylserine (PS) exposure.[2,7-9] Intriguingly, many of these diseases are also associated with protection from severe malaria,[10,11] which has led some authors to propose a role for RBC senescence and clearance in malaria resistance.[12-14]

RBC lifespan may be critically regulated by changes in intracellular adenosine nucleotide (adenosine triphosphate [ATP], adenosine 5′-diphosphate [ADP], and adenosine 5′-monophosphate [AMP]) levels.[15,16] For example, the shortened lifespan of RBCs in pyruvate kinase–deficient individuals and associated pathology has been linked to reduced RBC ATP levels. Similarly, ATP loss contributes to pathology in sickle cell disease.[17] Erythrocytic ATP levels are controlled by adenosine monophosphate deaminase (AMPD3), which converts AMP to inosine 5′-monophosphate (IMP) and plays an important role in maintaining the adenylate energy charge or the ratio of ATP to AMP. Thus, ATP loss may be mediated through AMPD3, which converts AMP to IMP. In most cells, the conversion of ITP back to AMP by adenylsuccinate synthetase and adenylsuccinate lyase balances AMPD3 activity. However, in RBCs, the machinery for conversion of IMP back to AMP is absent, and to maintain AMP/ATP levels, AMPD3 is inactivated. Reactivation of AMPD3 by oxidative stress has been linked to the ATP loss associated with RBC death.[18,19] As yet, it is unknown if AMPD3 plays an independent role in determining RBC lifespan.

Here, we report a novel, *N*-ethyl-*N*-nitrosourea (ENU)–induced mutation that causes a gain of function in AMDP3. Mice carrying the mutation exhibit reduced erythrocyte ATP, increased GTP, rapid RBC turnover with increased erythropoiesis, dramatically shortened RBC lifespan, and signs of increased RBC senescence. Mice were also found to be highly resistant to infection with the rodent malaria *Plasmodium chabaudi*.

Methods

For detailed methods, see supplemental Materials and methods (available on the *Blood* Web site).

Submitted August 31, 2015; accepted July 14, 2016. Prepublished online as *Blood* First Edition paper, July 27, 2016; DOI 10.1182/blood-2015-09-666834.

The online version of this article contains a data supplement.

The publication costs of this article were defrayed in part by page charge payment. Therefore, and solely to indicate this fact, this article is hereby marked “advertisement” in accordance with 18 USC section 1734.

Table 1. Hematological parameters of wild-type, MRI49372/+, and MRI49372 mice

	WT	MRI49372$^{m/+}$	MRI49372$^{m/m}$
WBC	9.6 ± 0.7	10.6 ± 0.5	20.2 ± 2.3**
RBC	10.3 ± 0.2	8.8 ± 0.4	5.9 ± 0.4***
HGB	106.1 ± 8.2	93.0 ± 7.7	71.2 ± 7.9**
MCV	53.1 ± 0.5	56.2 ± 0.4*	71.6 ± 2.1*
RDW	14.6 ± 0.2	14.1 ± 0.2	21.9 ± 1.0***
%Retic	2.3 ± 0.3	6.0 ± 1.1*	52.6 ± 6.5**
%Macro	0.3 ± 0.1	1.3 ± 0.3**	40.2 ± 5.5***
%Micro	0.4 ± 0.04	0.2 ± 0.01***	0.7 ± 0.1***
PLT	897.7 ± 48.7	962.9 ± 64.3	1181.4 ± 59.3*

Automated full blood analysis on WT (n = 15), SJL/J-*Ampd3*$^{T689A/+}$ (n = 21), and SJL/J-*Ampd3*^{T689A} (n = 14) mice. Values are mean ± SEM.

HGB, total hemoglobin g/L; MCV, mean corpuscular volume (fL); PLT, number of platelets 10^3 cells/μL; RBC, number of red blood cells × 10^6 cells/μL; RDW, percentage red cell distribution width; WBC, number of white blood cells × 10^3 cells/μL; %Macro, % macrocytic cells; %Micro, % microcytic cells; %Retics, % reticulocytes.

*$P < .05$; **$P < .01$; ***$P < .001$.

Animals

Mice were bred under specific-pathogen–free conditions. All procedures conformed to the National Health and Medical Research Council code of practice. Seven-week-old SJL male mice received intraperitoneal (IP) injections of 150 mg/kg ENU at 1-week intervals. Mutagenized G0 mice were crossed with background SJL. G1s were bled at 7 weeks for blood analysis. The G1 49372 mouse displayed a mean corpuscular volume 3 standard deviations higher than average; it was then crossed with SJL, and the resulting G2s were used for further experiments.

Whole-exome sequencing

DNA from 2 phenodeviant MRI49372 was isolated using a QIAGEN DNeasy blood and tissue kit (Hilden, Germany). ≥ 10 μg of DNA was prepared for paired-end genomic library using a kit from Illumina (San Diego, CA). Exome enrichment was performed using an Agilent Sure select kit. Samples were sequenced on a Hisequation 2000 platform. The variant calling and filtering methodology has been fully described elsewhere.[20] Briefly, we mapped the short sequence tags (reads) on the mouse genome (mm9/NCBI37) using BWA V0.61[21] and BOWTIE2.[22] Nucleotide variants were called using SAMTOOLS V0.1.19[23] and GATK.[24] From our variant filtration process, we retained those that are "common" and "private" to the 2 mutants, namely at an allelic frequency of 1 and not shared by other SJL mice and ENU mutant mice previously sequenced. Remaining variants were annotated using ANNOVAR.[25]

Complete blood count

Complete blood counts were obtained using an ADVIA 2120 hematology system. Reticulocyte count was determined by counting thin smears from tail blood stained in 10% Giemsa solution.

Western blots

Protein was separated by SDS-PAGE[26] using 8% gradient gels. Because the anti-AMPD3 antibody only recognizes native-state protein, lysates were not denatured prior to SDS-PAGE. Mouse monoclonal ACTB or rabbit polyclonal AMPD3 (Abcam) was used for immunoblotting. Band density was calculated using ImageJ.

Purine analysis

Magnetic activated cell sorting–separated mature RBCs ($CD71^-$), which were then washed in ice-cold PBS, and 20 μl packed cells were either snap frozen or incubated at 37°C, 50% hematocrit in Hank's balanced salt solution containing 2 mM AMP or 2 mM $^{13}C^{15}N$-U-AMP. Samples were collected at 0, 1, or 2 hours and washed in mouse tonicity phosphate-buffered saline. Packed cells were aliquoted and snap frozen. RBC aliquots were quenched and lysed in 200 μl ice-cold acetonitrile:water stable-isotope–labeled (^{13}C) internal standards. A ZIC-pHILIC LC-QTOF platform was used for global metabolome detection of mature RBCs. Untargeted data processing and statistical analysis were performed on the automated IDEOM pipeline.[27] Metabolite identification of purines was based on accurate mass, retention time, and authentic chemical standards, which is a level 1 standard of identification by the Metabolomics Standards Initiative.[28,29] Targeted analysis and isotope enrichment were determined by extraction of ion chromatograms based on accurate mass using MassHunter software (Agilent).

Erythropoiesis

Bone marrow and spleen cells from mutant and wild-type (WT) mice were stained with anti-TER119 and anti-CD44 (eBioscience). Cells were analyzed on a BD FACSARIA-II flow cytometer, recording 10 000 events per sample. Populations were gated as described previously.[30] A Quantikine mouse/rat immunoassay (R&D Systems) was used to measure plasma erythropoietin concentration according to the manufacturer's instructions. Plasma bilirubin was measured using TBIL strips on the VetTest Chemistry Analyzer (IDEXX Laboratories).

Half-life and senescence

RBC half-life was determined by IV administration of 1 mg NHS-biotin-ester dissolved in saline. Acute hemolysis was achieved by IP injection of 60 mg/kg phenylhydrazine on 2 consecutive days. After the second injection, blood was collected by tail snip each day for 7 days and stained with anti-TER119 and anti-CD71 (eBioscience). Cells were resuspended in mouse tonicity fluorescence-activated cell sorting containing 108 counting beads per microliter, and the number of $TER119^+CD71^-$ cells per bead was calculated. PS exposure, Ca^{2+} content, and reactive oxygen species (ROS) were measured by flow cytometry, in conjunction with Annexin V-FITC, FlUO3/AM, and H2DCFDA, respectively.

Nonheme iron

Liver and spleen tissue was dried at 45°C for 48 hours and then placed in a 10% hydrochloric acid/10% trichloroacetic acid solution to digest for 48 hours at 65°C. Samples were centrifuged, and 200 μl supernatant was added to 1 ml 1,10-phenanthroline monohydrate solution and incubated for 15 minutes at room temperature. After incubation, absorbance was measured at 508 nm.

Osmotic fragility

Blood was incubated 1:100 in NaCl solutions ranging from 0 to 160 mmol. After 30 minutes at 37°C, samples were centrifuged and the absorbance of the supernatant measured at 545 nm. Percentage lysis was calculated by comparison with 100% lysis at 0 mmol NaCl.

Lysis in culture

Blood was incubated 1:100 in supplemented RPMI at 37°C for 24 hours. Samples were centrifuged, and supernatant was collected for analysis by absorbance at 545 nm. The percentage of cells lysed was calculated by comparison with samples that were completely lysed by freezing and thawing.

Infections

Experiments used either the rodent parasite *P. chabaudi adami DS (408XZ)* or *P. berghei ANKA*. Parasite stocks were prepared from passage through resistant C57BL/6 and SJL/J mice, respectively, as described previously.[31] Experimental mice were infected with an IP dose of 1 × 10^4 parasitized RBCs. Blood stage parasitemia was determined by taking thin smears from tail blood (1 μl per day from days 7-14 postinfection) stained in 10% Giemsa solution. The percentages of infected reticulocytes and infected mature red cells were calculated.

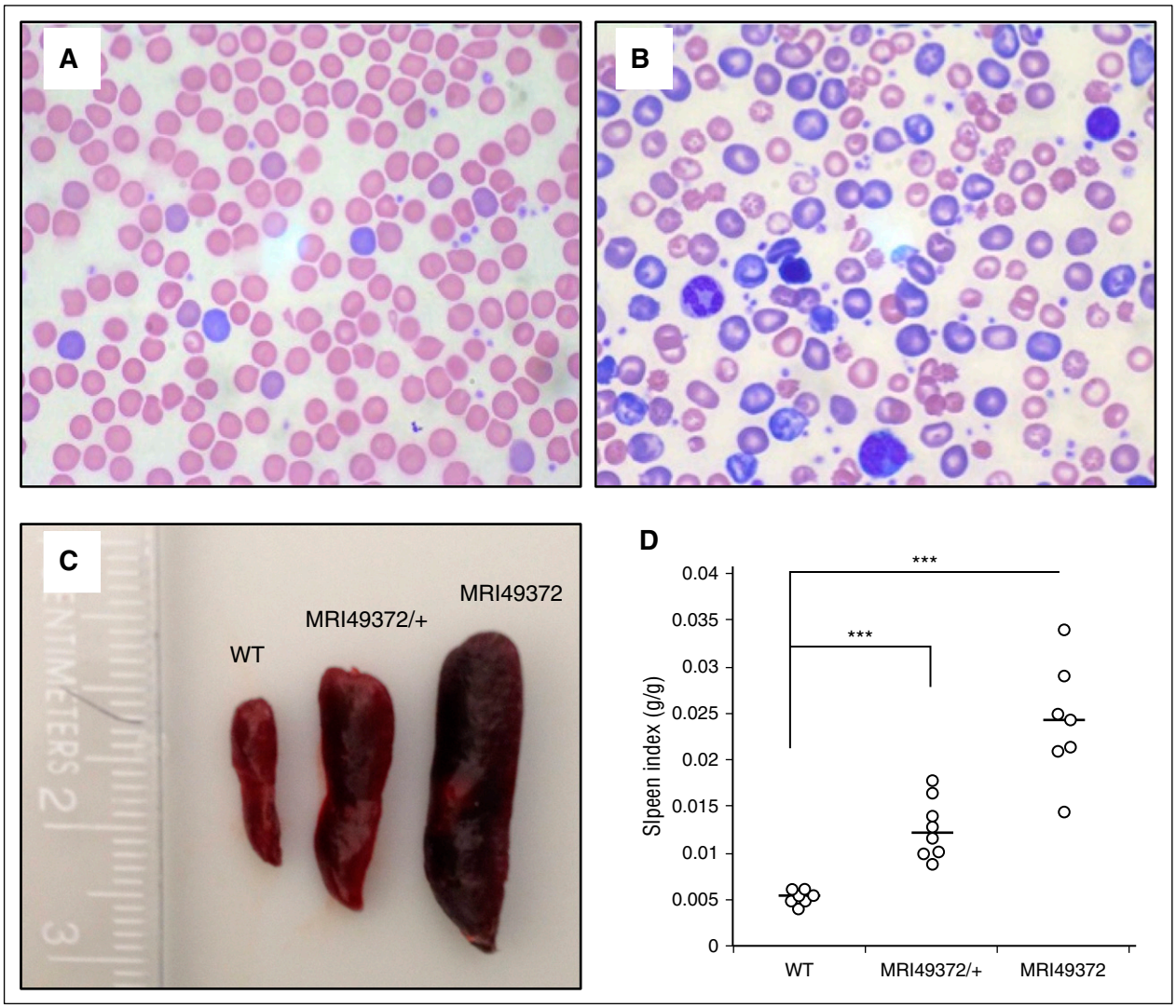

Figure 1. MRI49372 macrocytic anemia and splenomegaly. (A) Representative light microscopy image of Wright-Giemsa–stained WT thin smear. (B) Representative light microscopy image of Wright-Giemsa–stained *Ampd3*^{T689A} thin smear. (C) Representative spleens from WT, MRI49372/+, and MRI49372 mice. (D) Spleen index, calculated as spleen weight (g)/mouse weight (g) for WT (n = 7), MRI49372/+ (n = 8), and MRI49372 (n = 7). Black bars represent median. ***$P < .001$. *P* values calculated using the Student *t* test.

Results

MRI49372 founders display a macrocytic anemia

In screen looking for dominant ENU-induced novel malaria/red cell phenotypes, we identified a G1 animal (MRI49372) with leukocytosis, thrombocytosis, reticulocytosis, macrocytosis, and anisocytosis, accompanied by moderate anemia. We confirmed that this phenotype was heritable by progeny testing. Intercrossing 2 affected G2 mice produced the WT phenotype in 25% of progeny, the G1 founder phenotype in 50% (therefore heterozygotes [MRI49372/+]), and a more severe abnormal blood phenotype in the last 25% (homozygote for causative mutation [MRI49372]) (Table 1). Wright-Giemsa–stained blood smears of the more severe phenotype confirmed a macrocytic anemia and also showed increased target cells, blister cells, acanthocytes, polychromasia (Figure 1A-B), and elevated reticulocyte and platelet counts (Table 1). The MRI49372 phenotype is consistent with a hemolytic anemia. Mutants also exhibited significant splenomegaly, with a twofold increase in spleen index in MRI49372/+ and a fourfold increase in spleen index in MRI49372 (Figure 1C-D).

Whole-exome sequencing of 2 homozygous G3 animals identified 9 mutations common to both animals. In order to identify the

Table 2. List of nonsynonymous gene candidates held in common between both mutants sent for whole-exome sequencing

Chromosome	Location	Base		Gene name	LOD score	n
		Ref	Var			
7	81356970	A	T	*Cpeb1*	0.69	32
7	114536169	A	T	*Pde3b*	2.58	21
7	110809847	A	G	*Ampd3*	6.55	22
7	104260195	G	A	*Trim34a*	0.51	11
6	40680762	C	T	*Mgam*	0	6
1	119678820	T	G	*Ptpn4*	1.19	4
12	72652426	T	A	*Dhrs7*	0.23	4
13	81521252	C	G	*Gpr98*	1.19	4
16	29409849	T	A	*Atp13a4*	0.23	4

LOD, logarithm of the odds; Ref, reference; Var, variant.

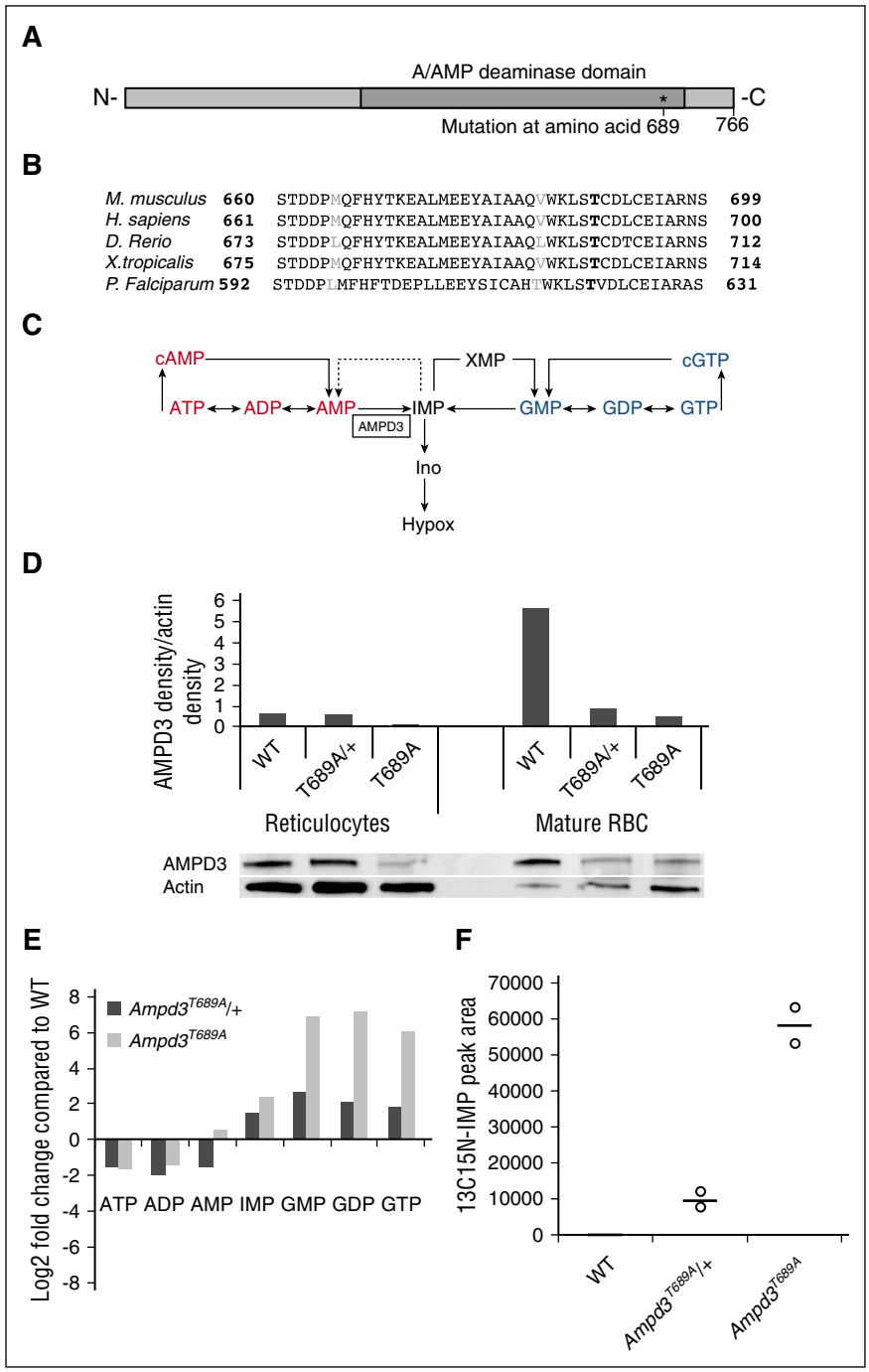

Figure 2. The MRI49372 phenotype is caused by a mutation in *Ampd3*. (A) Representation of the position of the mutation within the protein. (B) Sequence alignment showing conserved residues in AMPD3. Black letters represent residues conserved in 4/5 listed species. Bold "T" is the position of the *Ampd3*^{T689A} mutation. (C) Simplified diagram of purine metabolism showing reaction catabolized by AMPD3. Dotted line indicates reaction that does not proceed in human RBCs. It is not known if this reaction proceeds in mouse RBCs. cAMP, cyclic AMP; cGTP, cyclic GTP; GDP, guanosine 5′-diphosphate; GMP, guanosine 5′-monophosphate; GTP, guanosine 5′-triphosphate; Hypox, hypoxanthine; Ino, inosine; XMP, xanthosine 5′-monophosphate. (D) Representative western blot of (magnetic-activated cell sorting) separated reticulocytes (CD71^{+}) and mature RBCs (CD71^{-}) showing AMPD3 for WT, *Ampd3*$^{T689A/+}$, and *Ampd3*^{T689A}, as well as actin loading control for the same blot. Graph shows AMPD3 band density relative to actin band density (E). Mean ± standard of the mean (SEM) fold change in purine concentration in mature RBCs (CD71^{-}) for *Ampd3*$^{T689A/+}$, and *Ampd3*^{T689A} compared with WT. Data show average of technical replicates (n = 4) from pooled biological replicates (n = 6). (F) Accumulation of $^{13}C/^{15}N$-labeled IMP in mature WT, *Ampd3*$^{T689A/+}$, and *Ampd3*^{T689A} RBCs (CD71^{-}) incubated at 37°C for 2 hours with labeled AMP. Data points represent technical replicates from pooled biological replicates (n = 3); black bars indicate median.

causative mutation, N2 mice were generated by crossing phenodeviant MRI49372 mice to BALB/c, and polymorphic single-nucleotide polymorphisms were genotyped. 12/13 affected mice were heterozygous across three chromosome 7 single-nucleotide polymorphisms, giving a logarithm of the odds score of 2.38 and suggesting a link between blood phenotype and this region of the genome (supplemental Figure 1). The 4 candidate mutations within this region were sequenced in a larger cohort of MRI49372, and it was found that the A-to-G base substitution in *Ampd3* at location 7:117953361 associated completely with the abnormal blood phenotype (Table 2). The mutation causes a substitution of alanine for threonine at position 689 in the AMPD3 protein (Figure 2A). Therefore, the allele has been termed *Ampd3*^{T689A}, and the strain is SJL/J-*Ampd3*^{T689A}. This mutation is predicted to disrupt an α helix within the highly conserved catalytic site of the protein (Figure 2B; supplemental Figure 2). Although the WKLSTCD motif containing the residue is a predicted phosphorylation site, 2D western blot analysis showed no evidence that AMPD3 phosphorylation was altered in mutant mice (supplemental Figure 3).

The Ampd3^{T689A} mutation causes an activation of *AMPD3*

AMPD3 is the erythrocyte-specific isoform of AMP deaminase; it catalyzes the hydrolytic deamination of adenosine monophosphate to IMP, a branch point in the adenylate catabolic pathway (Figure 2C). It is tightly regulated and helps to maintain ATP levels and the cellular

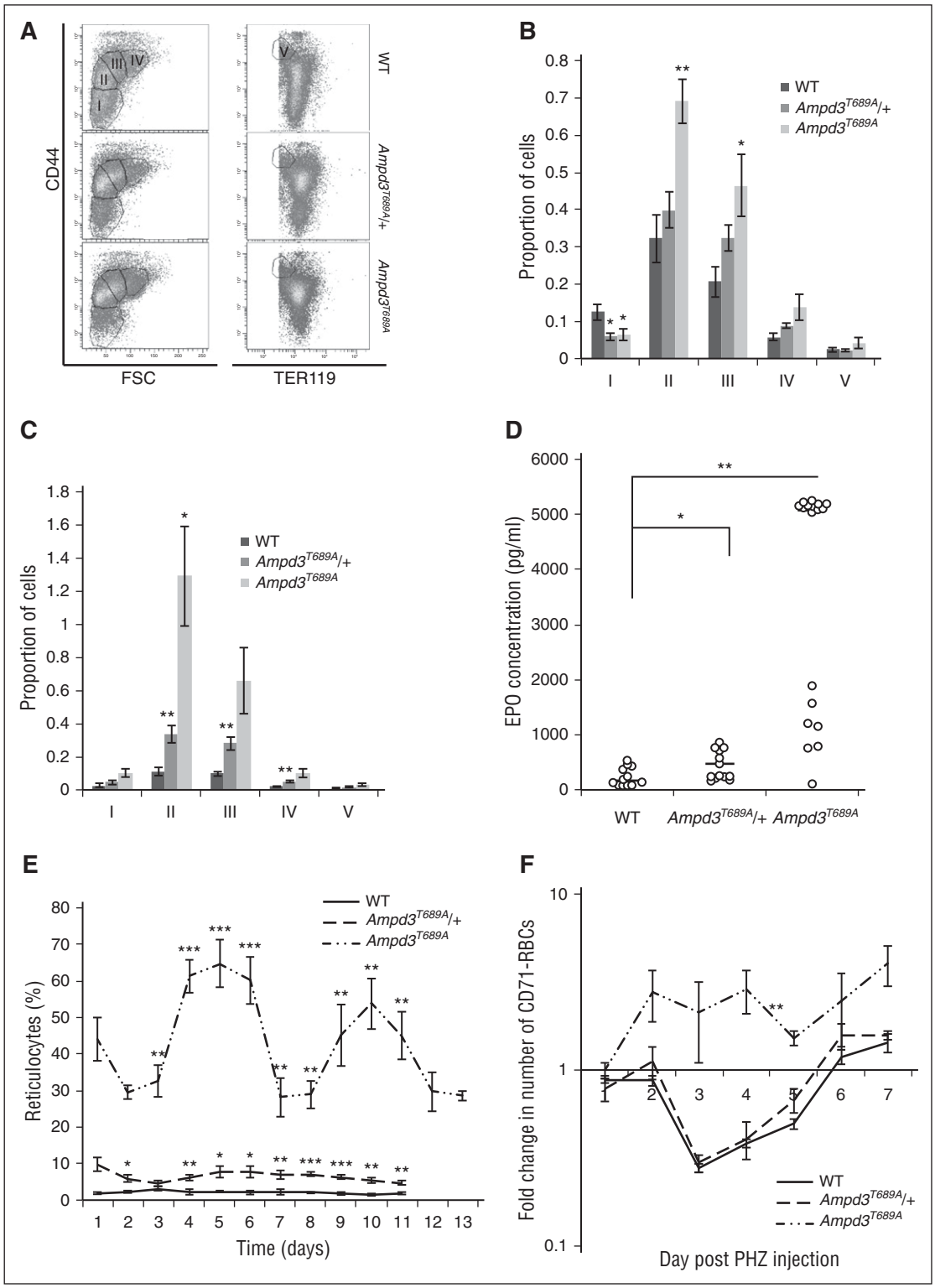

Figure 3. *Ampd3*^{T689A} has elevated erythropoiesis. (A) Representative plots showing the flow cytometry gating strategy using CD44 and TER119 staining. Proportion of TER119^{+} erythroblast populations in the (B) bone marrow and (C) spleen, calculated relative to the number of TER119^{-} cells, for WT, *Ampd3*$^{T689A/+}$, and *Ampd3*^{T689A}. I, RBCs; II, reticulocytes; III, polychromatic erythroblasts; IV, basophilic erythroblasts; V, proerythroblasts. (D) EPO concentration in the plasma of WT, *Ampd3*$^{T689A/+}$, and *Ampd3*^{T689A}. Black bars represent median. (E) Mean ± SEM percentage peripheral reticulocytes in WT (n = 4), *Ampd3*$^{T689A/+}$, (n = 8), and *Ampd3*^{T689A} (n = 5) mice over the course of 11 days. Values from *Ampd3*^{T689A} have been adjusted so that the peaks of reticulocytosis align. (F) Fold change compared with day 0 in number of CD71^{-} RBCs on day 1-7 after phenylhydrazine (PHZ) injection for WT (n = 5), *Ampd3*$^{T689A/+}$ (n = 4), and *Ampd3*^{T689A} (n = 4). Values are average ± SEM. *$P < .05$; **$P < .01$; ***$P < .001$. *P* values calculated using the Student *t* test.

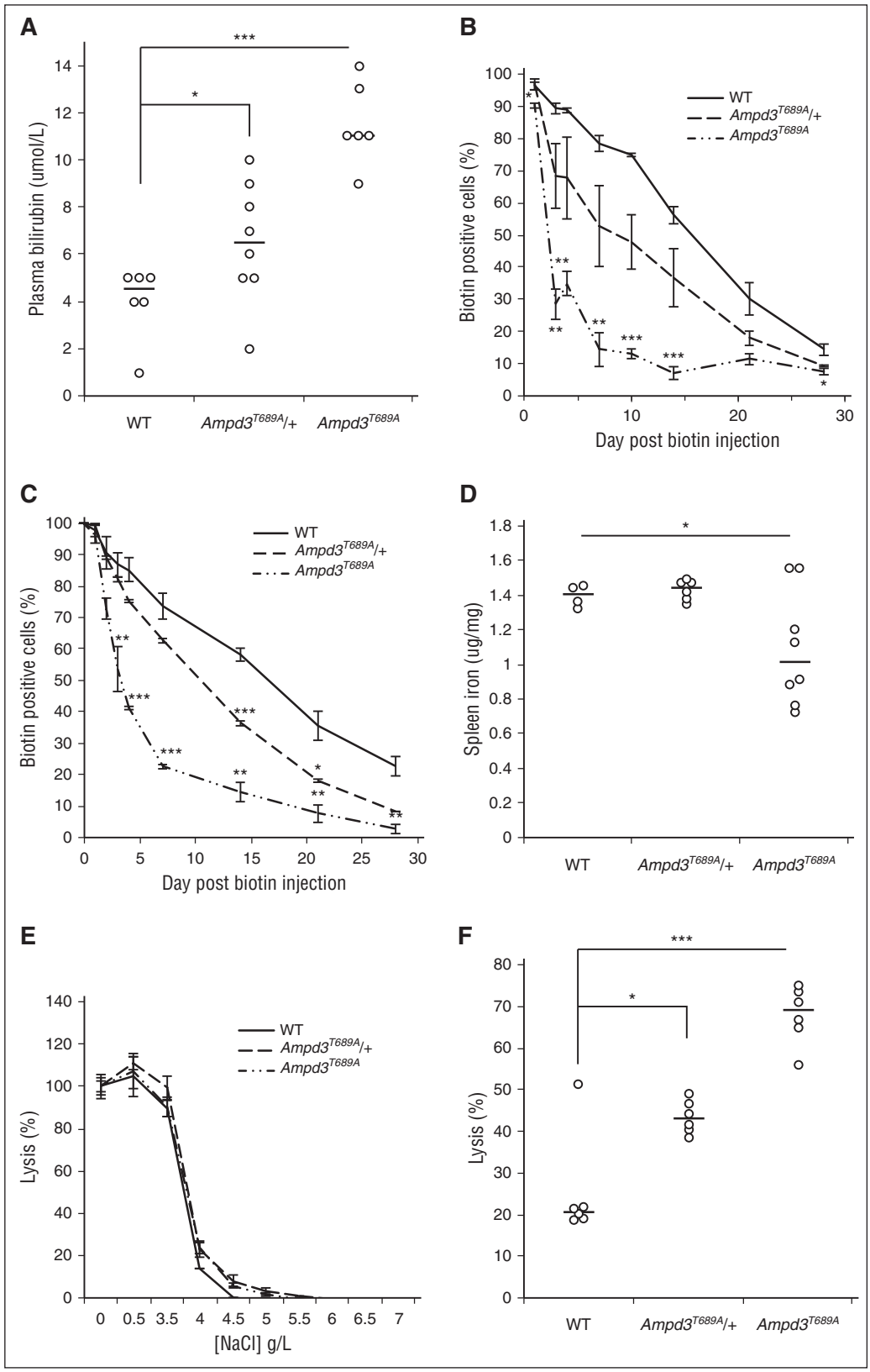

Figure 4. The *Ampd3*^{T689A} mutation shortens erythrocyte lifespan. (A) Amount of bilirubin in the plasma of WT, *Ampd3*$^{T689A/+}$ and *Ampd3*^{T689A} mice. Black bars indicate median. (B) RBC half-life in WT, *Ampd3*$^{T689A/+}$ and *Ampd3*^{T689A} mice, as measured by loss of biotinylated cells from circulation. (C) RBC half-life in splenectomized WT, *Ampd3*$^{T689A/+}$, and *Ampd3*^{T689A} as measured by loss of biotinylated cells from circulation. (C) Amount of nonheme iron (in duplicate) in the spleen of WT (n = 2), *Ampd3*$^{T689A/+}$ (n = 2), and *Ampd3*^{T689A} (n = 4). Black bars indicate median. (D) Osmotic fragility of WT, *Ampd3*$^{T689A/+}$, and *Ampd3*^{T689A} (all genotypes n = 3). (F) Amount of lysis for WT, *Ampd3*$^{T689A/+}$ and *Ampd3*^{T689A} cells incubated in vitro at 37°C for 24 hours, measured by absorbance at 545 nm, and compared with 100% lysis. Values are mean ± SEM. *$P < .05$; ***$P < .001$. *P* values calculated using the Student *t* test.

adenylate pool. Reverse-transcription polymerase chain reaction in embryonic day 14 livers showed a modest (1.5-fold) increase in *Ampd3* transcript in homozygous mutants (supplemental Figure 4). In contrast western blotting showed a decrease in AMPD3 abundance in reticulocytes ($CD71^+$) and mature RBCs ($CD71^-$) (Figure 2D), as well as embryonic day 14 livers (supplemental Figure 4). The relative abundances of ATP, ADP, AMP, IMP, guanosine monophosphate (GMP), guanosine diphosphate (GDP), and guanosine triphosphate (GTP) in mature RBCs were assayed by liquid chromatography-mass spectrometry. Heterozygous cells contained approximately half the levels of ATP, ADP, and AMP of WT cells but more than double the amount of IMP, GMP, GDP, and GTP. Homozygote cells were similarly deficient in ATP and ADP (but not AMP) and had more striking increases in IMP (5.3-fold), GMP, GDP and GTP (>50-fold) (Figure 2E). These results suggest the mutation results in a more enzymatically active form of AMPD3; ie, a gain-of-function mutation . To confirm this, mature RBCs were incubated with labeled $^{13}C^{15}N$-uniformly labeled AMP, and the accumulation of $^{13}C^{15}N$-IMP and $^{13}C^{15}N$-ADP was measured over a period of 4 hours. No $^{13}C^{15}N$-IMP production was observed in WT mice. However, significant levels of the IMP isotope were detected in heterozygous cells, and even greater levels (sixfold) were found in homozygous cells (Figure 2F). To confirm that the increased synthesis of $^{13}C^{15}N$-IMP was not due to increased uptake of $^{13}C^{15}N$-ADP (which was also increased in *Ampd3*^{T689A} cells), RBC lysates were incubated with $^{13}C^{15}N$-ADP. As in live cells, increased synthesis of IMP was observed in *Ampd3*^{T689A} RBC lysates compared with WT RBCs (supplemental Figure 5).

The Ampd3^{T689A} mutation decreases RBC lifespan

To understand the cause of macrocytosis and reticulocytosis mediated by the *Ampd3*^{T689A} mutation, erythropoiesis was investigated. Significantly higher proportions of erythroblasts were observed in the spleen and bone marrow, and significantly higher concentrations of erythropoietin were found in the plasma of mutant mice (Figure 3D), indicating elevated erythropoiesis. Interestingly, homozygous mutants displayed oscillatory reticulocytosis, fluctuating from 20% to 80% over a 5-day cycle (Figure 3E). Following induction of an acute anemia (phenylhydrazine injection), both WT and heterozygous mice showed similar rates of recovery in red cell numbers. The already highly depressed erythrocyte levels in the homozygous mice were not significantly reduced by treatment and instead increased in the days following (Figure 3F), suggesting that the elevated erythropoiesis in homozygous mice can outpace the destruction caused by PHZ.

Elevated erythropoiesis, hyperbilirubinemia, and erythropenia characterize erythrocytic destruction. In support of this hypothesis, a significant increase in plasma bilirubin was observed in mutants (Figure 4A). Erythrocytic half-life was significantly reduced in the heterozygote (8.5 days) and homozygote (2.5 days) strains compared with the WT (15.5 days) (Figure 4B). The RBC half-life in splenectomized mice was similarly reduced (Figure 4C), indicating that the spleen was not the major mediator of RBC destruction in mutant mice. Furthermore, splenic iron levels were not elevated in the mutant mice, as assessed by Perl's blue staining (supplemental Figure 6) or by measuring total nonheme iron (Figure 4D), although lower nonheme iron was observed in homozygous spleens, which may indicate iron deficiency related to excessive hemolysis. In addition, no differences in osmotic fragility were observed between mutant and WT blood (Figure 4E). As an alternative to increased splenic destruction, we determined if the mutant RBCs were more susceptible to spontaneous lysis. Following ex vivo incubation for 24 hours at 37°C, >40% and 70% of heterozygous and homozygous blood cells, respectively, were lysed, compared with only 20% of WT cells. (Figure 4F). We next isolated mature red cells ($CD71^-$) and measured expression of markers of cell senescence. Compared with WT, significantly higher levels of ROS and intracellular Ca^{2+} were observed in mutant cells, and significantly higher levels of PS exposure were observed heterozygous, but not homozygous, cells (Figure 5). Together, these results indicate that the shortened lifespan of *Ampd3*^{T689A} RBCs is determined by erythrocyte-autonomous factors and not the spleen. Given elevated PS exposure is not observed in homozygous cells, it may not play a major role in the observed hemolysis.

Ampd3^{T689A} mice are resistant to erythrocytic-stage *P. chabaudi* infection

Shortened RBC half-life is observed in many diseases known to provide resistance to malaria, including hemolytic anemia, sickle cell disease, thalassemia, G6PD deficiency, and hereditary spherocytosis.[6] To test if the *Ampd3*^{T689A} conferred a similar malaria resistance phenotype, we challenged homozygous, heterozygous, and WT mice with *P. chabaudi*. Indeed, 100% of the homozygous and 60% of the heterozygous animals survived infection, whereas all the WT animals died (Figure 6A); the survival phenotype also correlated with 90% and 50% reductions in peak parasitemia, respectively (Figure 6B). In contrast, infection of the mutant mice with the reticulocyte preferring *P. berghei* species did not result increased survival (supplemental Figure 7C-D). A comparison of reticulocyte infection rates in both species indicated no significant differences (supplemental Figure 7A-B), collectively indicating that the large percentage of reticulocytes in mutant mice was not a barrier to the development of high parasitemia. During these experiments, it was also observed that significantly more *P. berghei* gametocytes were present in mutant mice (supplemental Figure 8); these gametocytes were also able to undergo complete development in the mosquito and infect new mice (data not shown).

To determine if the reduced *P. chabaudi* parasitemia was the result of RBC-autonomous factors, an in vivo invasion and growth assay was conducted.[31] Blood from *Ampd3*$^{T689A/+}$ and WT mice was labeled with different fluorescent markers, mixed in equal proportions, and injected into *P. chabaudi*–infected WT mice while parasites were undergoing schizogony. The parasitemia of each labeled population was monitored over 21 hours to determine differences in parasite invasion and development. Parasites were detected by staining RNA (thiazole orange) and DNA (Hoechst). After 12 hours, 2 populations were visible: thiazole orange^{low}/Hoescht^{low} and thiazole orange^{high}/Hoescht^{high}, which likely represent RBCs containing the ring stage and trophozoite stage of parasite development, respectively.

At all time points, more parasites were observed in *Ampd3*$^{T689A/+}$ than WT cells (Figure 6C). Although this difference was modest (10%), it was significant at both 3 and 12 hours. At 12 hours, a statistically significant increase in the proportion of trophozoites was observed in heterozygous cells compared with WT cells, almost double that of WT cells (39% vs 20% in *Ampd3*$^{T689A/+}$ cells) (Figure 6D). Together, these results suggest that the environment within *Ampd3*$^{T689A/+}$ RBCs does not impede *P. chabaudi* growth and, according to the parasite development data, may even favor a faster rate of development. This was further supported by the observation that human RBCs with artificially elevated GTP levels supported normal growth of *Plasmodium falciparum* (supplemental Figure 9).

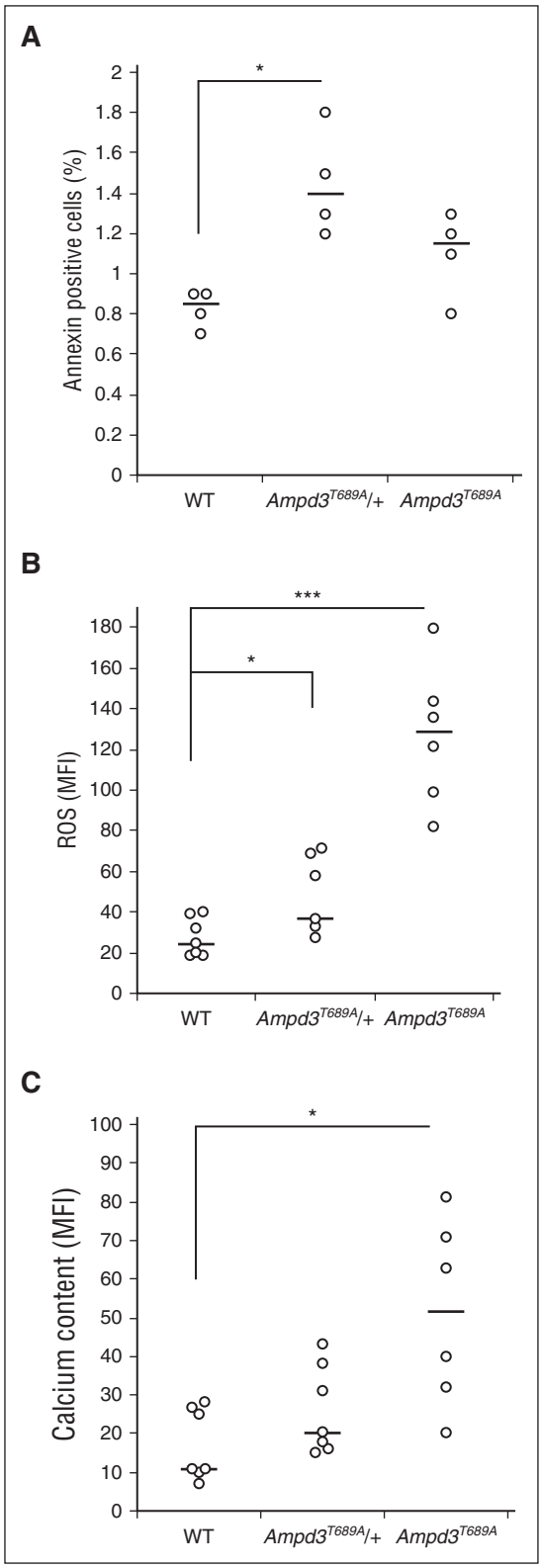

Figure 5. The *Ampd3*^{T689A} mutation causes increased oxidative stress and cell senescence. (A) Proportion of Annexin V–positive mature RBCs (CD71$^-$) (n = 4). (B) Amount of reactive oxygen species in mature RBCs (CD71$^-$) as measured by mean fluorescence intensity of H_2DCFDA, for WT (n = 7), *Ampd3*$^{T689A/+}$ (n = 7), and *Ampd3*^{T689A} (n = 6). Combined results of 2 independent experiments are shown. (C) Amount of calcium in mature RBCs (CD71$^-$) as measured by mean fluorescence intensity of FLUO3-am for WT (n = 7), *Ampd3*$^{T689A/+}$ (n = 7), and *Ampd3*^{T689A} (n = 6). Combined results of 2 independent experiments are shown. Black bars represent median. *$P < .05$; ***$P < .001$. *P* values calculated using the Student *t* test.

The Ampd3^{T689A} mutation stimulates reticulocytosis during infection

Mice carrying the *Ampd3*^{T689A} allele exhibit splenomegaly, which is positively correlated with malaria resistance.[32,33] Therefore, it is possible that the spleen mediates malaria resistance in the *Ampd3*^{T689A} line. To investigate this, female mice were splenectomized and then infected with *P. chabaudi.* There was a significant delay to death in the homozygous mice compared with splenectomized WT mice (up to 4 days) (Figure 7A). Peripheral parasitemia levels were significantly reduced in both mutant types compared with WT, which is equivalent to that observed in nonsplenectomized animals (Figure 7B).

Severe anemia is one of the major causes of morbidity and mortality during *Plasmodium* infection.[34] Given that *Ampd3*^{T689A} mice have increased erythropoiesis when uninfected, it was thought possible that a more brisk erythropoietic response may mediate their increased survival. Reticulocyte levels were monitored daily over the course of *P. chabaudi* infection in both splenectomized and nonsplenectomized female mice. In nonsplenectomized mice, *Ampd3*$^{T689A/+}$ increased reticulocyte levels from 10% to 58% over the course of infection. Despite displaying a similar level of anemia (supplemental Figure 10) early in infection, nonsplenectomized WT mice maintained reticulocyte levels at 5%. In *Ampd3*^{T689A} nonsplenectomized mice, reticulocytes remained at 50% (Figure 7C). In splenectomized mice, the reticulocytes level was unchanged for WT but altered for both splenectomized mutants; reticulocyte levels remained steady in *Ampd3*$^{T689A/+}$ splenectomized mice and fell from 43% to 19% in splenectomized *Ampd3*^{T689A} mice (Figure 7D). These results show that nonsplenectomized *Ampd3*$^{T689A/+}$ mice are able to increase erythropoiesis in response to *P. chabaudi* infection and the nonsplenectomized *Ampd3*^{T689A} mice reticulocytosis level remained high throughout the course of the infection. This increase or high reticulocytosis level may help alleviate anemia and increase survival.

Discussion

The MRI49372 blood phenotype is caused by a gain-of-function mutation in Ampd3

A mutation in *Ampd3* in the MRI49372 line completely cosegregates with the MRI49372 hematological phenotype. This mutation is associated with an increase in the rate of conversion of erythrocytic AMP to IMP. In the absence of identified cosegregating exonic mutations, we conclude that the MRI49372 blood phenotype is caused by a gain-of-function mutation in *Ampd3* that causes increased flux through the AMPD3 enzyme.

AMPD3 catalyses the conversion of AMP to IMP, providing an important pathway for maintaining ATP levels within RBCs. In most cell types, IMP can be converted back to AMP in a 2-step process catalyzed by adenylosuccinate synthase and adenylosuccinate lyase. However, adenylosuccinate synthase is inactive in human (and presumably mouse) erythrocytes, preventing AMP salvage via this pathway.[35,36] AMPD3 is therefore normally repressed in human RBCs to prevent irreversible loss of ATP, hemolysis, and anemia.[16] The results from our experiments with labeled AMP suggest that AMPD3 activity is similarly repressed in normal mouse erythrocytes under normal circumstances. The MRI49372 mutation relieves this repression.

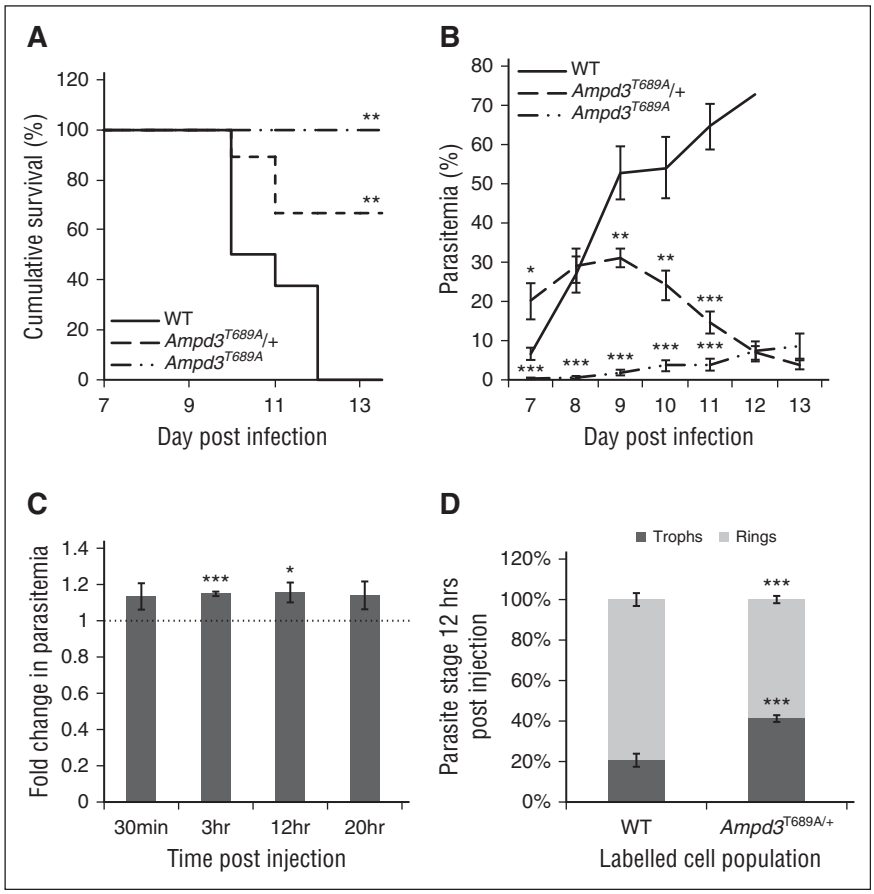

Figure 6. The *Ampd3*^{T689A} mutation causes an altered response to malaria. Cumulative survival (A) and peripheral parasitemia (B) for female WT (n = 17), *Ampd3*$^{T689A/+}$ (n = 11), and *Ampd3*^{T689A} (n = 6) infected with *P. chabaudi*. (C) Mean ± SEM fold change in parasitemia compared with WT for *Ampd3*$^{T689A/+}$ labeled RBCs. Dotted line indicates equal ratio of WT to mutant. (B) Mean ± SEM proportion of ring stage (thiazole orange^{low}, Hoechst^{low}), and trophozoite stage (thiazole orange^{high}, Hoechst^{high}) parasites within labeled WT and *Ampd3*$^{T689A/+}$cells (n = 7). *$P < .05$; **$P < .01$; ***$P < .001$. *P* values calculated using the log-rank test (survival) or the Student *t* test.

Ampd3^{T689A} has a shortened RBC half-life

Erythrocyte half-life was significantly shortened in *Ampd3*^{T689A} mutants. This could be due to a defect in red cell maturation, increased RBC destruction, or a combination of both. The presence of elevated reticulocytes with low numbers of mature RBCs in the *Ampd3*^{T689A} strain is suggestive of increased destruction; this could be mediated either by excessive splenic clearance or by spontaneous lysis due to intrinsic red cell factors. In hereditary spherocytosis, a disorder where changes to membrane deformability cause excessive destruction of RBCs in the spleen, the resulting chronic hemolysis and shortened RBC half-life can be improved by partial splenectomy.[37] As splenectomy only marginally increased the RBC half-life in *Ampd3*^{T689A} mice, it can be assumed that aberrant splenic clearance is not the major cause of hemolysis. Given that mutant RBC lifespan is also decreased in vitro, cell-intrinsic factors are most likely to determine the decreased RBC lifespan.

No studies have yet investigated directly whether AMPD3 has a role in programmed RBC death. However, a number of observations from this study suggest that *Ampd3*^{T689A} erythrocytes are undergoing accelerated senescence; they have increased intracellular calcium, PS exposure (in *Ampd3*$^{T689A/+}$), and an increased proportion of microcytic cells. They also exhibit a decreased concentration of adenosyl nucleotides and significantly increased amounts of ROS, both of which can trigger erythrocytic death.[38] Taken together, these observations suggest the following mechanism of reduced RBC half-life: activation of AMPD3 causes depletion of ATP and loss of ATP-dependent oxidative defense metabolism, which in turn increases oxidative stress. Increased oxidative stress then triggers Ca^{2+} influx, cell shrinkage, PS exposure, and cell death.

Another novel finding of this study is that *Ampd3*^{T689A} mice display cyclic reticulocytosis, which oscillates between 20% and 80% over a 5-day cycle. Although spontaneous oscillatory reticulocytosis has not previously been described in mice, similar phenotypes have been observed in several clinical conditions, including cyclic neutropenia, periodic chronic myelogenous leukemia, cyclic thrombocytopenia, and periodic autoimmune hemolytic anemia.[39-41] In comparison with these conditions, the oscillations observed in *Ampd3*^{T689A} are remarkably short. Most other hematologic oscillatory behaviors range from 12 to 80 days.[41] For some of these conditions, the causes of pathology have been identified,[40,42-44] but these do not always explain why oscillations occur.[45] *Ampd3*^{T689A} may therefore provide a useful model for investigating the underlying causes of cyclic hematopoiesis.

Ampd3^{T689A} may cause malaria resistance through high RBC turnover

This study provides the first evidence that host AMPD3 has a role in the response to malaria infection. Although AMPD3 activation has previously been shown to contribute to the pathology of sickle cell disease,[17] a condition well known to provide malaria resistance, this study is the first study to provide a direct link between malaria infection and AMPD3 activation. It shows that activation of AMPD3 dramatically increases resistance to *P. chabaudi* infection, characterized by significant reductions in peak parasitemia and increased rates of survival. In homozygous mutants, low parasitemia may be explained by the short RBC half-life. Both splenectomized and nonsplenectomized *Ampd3*^{T689A} mice lose a quarter of their RBCs every day, and this phenotype may be exacerbated during infection.[46] Therefore, in these

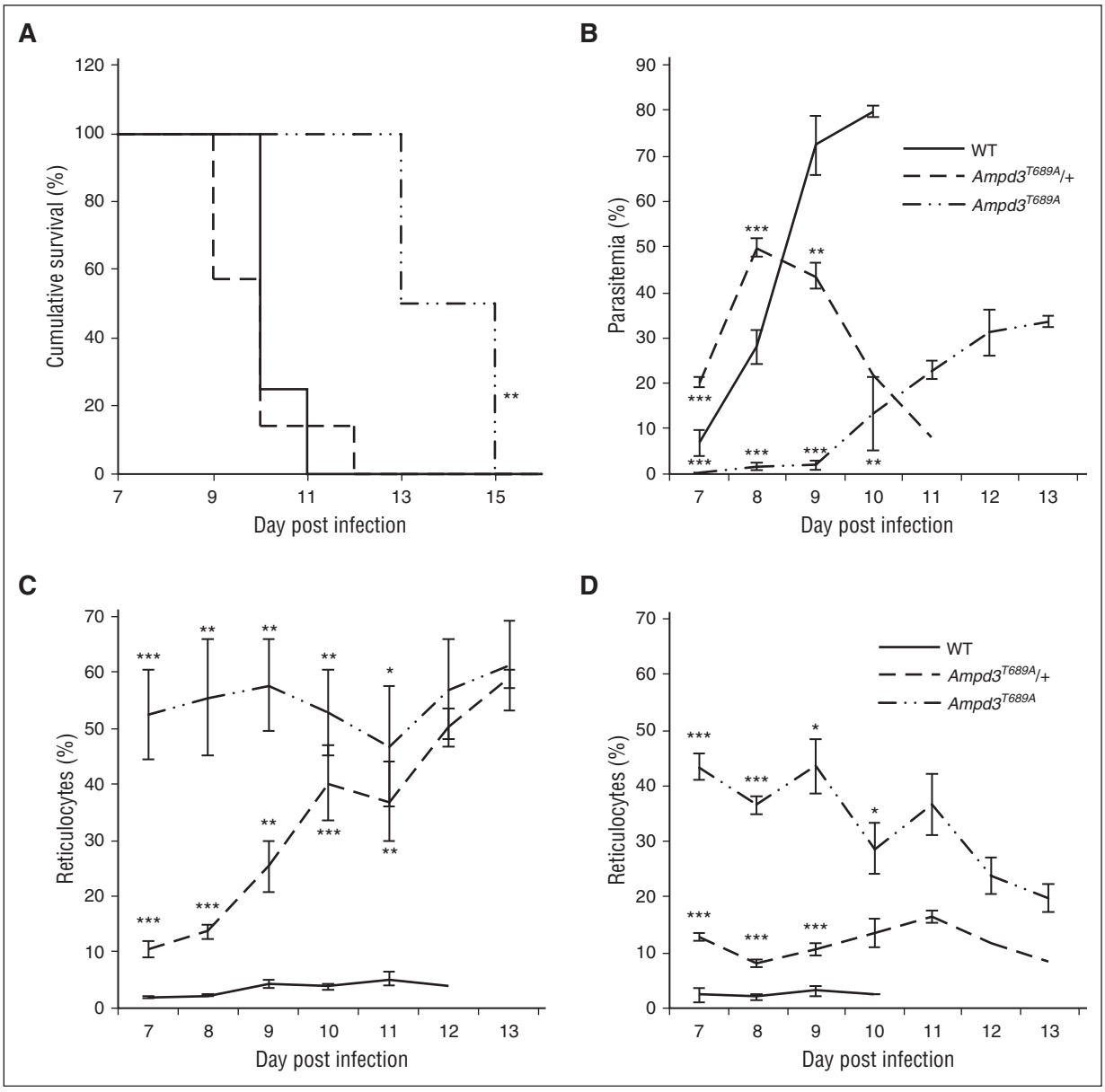

Figure 7. Ampd3^{T689A} has altered reticulocytosis in response to infection and splenectomy. Cumulative survival (A), peripheral parasitemia (B), and reticulocyte response (C-D) for splenectomized (A-B,D) or nonsplenectomized (C) female mice. (A-B,D) WT (n = 8), *Ampd3*$^{T689A/+}$ (n = 8), and *Ampd3*^{T689A} (n = 4) infected with *P. chabaudi*. Mean ± SEM proportion of reticulocytes and parasitemia in (C) *P. chabaudi*–infected female WT (n = 17), *Ampd3*$^{T689A/+}$ (n = 11), and *Ampd3*^{T689A} (n = 6) mice. $^{*}P < .05$; $^{**}P < .01$; $^{***}P < .001$. *P* values calculated using the Student's *t* test.

animals, a large proportion of merozoites may invade cells that will not survive the full 24 hours the parasite needs to complete replication.

There are many similarities between *Ampd3*^{T689A} and other genetic conditions known to provide malaria resistance. For example, pyruvate kinase, sickle cell disease, G6PD, and thalassemia all show shortened RBC half-life, increased reticulocytes, low RBC ATP, and increased oxidative stress. In each case, a number of mechanisms have been proposed for the observed resistance, including decreased invasion, decreased parasite growth, and increased RBC senescence.[10] Although all processes may contribute to resistance, *Ampd3*^{T689A} highlights that a short half-life can have a large impact on the course of parasitemia, even when parasite invasion rates are unaffected and parasite growth rates are increased.

Our results showed that AMPD3 is critical to maintain the ATP within RBCs. The fact that higher parasitemia was observed in Ampd3$^{T689A/+}$ early in *P. chabaudi* infection suggested that the Ampd3^{T689A} mutation causes RBC-autonomous effects that favor parasite growth (Figure 6B). This was further supported by the in vivo invasion assay, which showed that *P. chabaudi* is able to both invade Ampd3$^{T689A/+}$ cells more easily and grow faster within them (Figure 6C-D). We hypothesized GTP could be the effector of this parasite growth. Further, in vitro assays with *P. falciparum* and human red cells confirmed that GTP is able to increase parasite growth in a dose-dependent manner (supplemental Figure 9). Therefore, we excluded the role of GTP as an effector mechanism for malaria resistance and reduced red blood cell half-life.

In summary, our results demonstrate that AMPD3 is important for regulating the lifespan of RBC. Its activation causes loss of intracellular ATP levels and rapid RBC senescence and turnover.

This, in turn, provides dramatic resistance to *P. chabaudi* and highlights the importance of RBC lifespan in controlling malaria. Our research suggests activating erythrocytic AMPD3 as a therapeutic approach to stimulate erythropoiesis during malaria infection.

Acknowledgments

The authors thank Noel Davies for his initial work measuring ATP and GTP in the samples, Elizabeth Tegg for staining some slides, and Meredith Roberts-Thompson for running samples on the Advia. The authors also thank three anonymous reviewers for their insightful comments on the manuscript.

This work was supported by the National Health and Medical Research Council of Australia (program grant 490037 and project grants 605524 and APP1047090), the Australian Society for Parasitology, OzEMalaR, National Collaborative Research Infrastructure Strategy, the Education Investment Fund from the Department of Education and Training, the Australian Phenomics Network, the Howard Hughes Medical Institute, and the Bill and Melinda Gates Foundation.

Authorship

Contribution: E.H., B.N., D.T., D.C.B., S.B.A., M.J.M., I.A.C., B.J.M., S.J.F., and G.B. designed research; E.H., B.N., D.C.B., L.M.J., I.A.C., S.L., and G.B. performed research; E.H., B.N., I.A.C., and G.B. contributed vital reagents; E.H., B.N., D.T., I.A.C., D.C.B., M.J.M., B.J.M., S.J.F., and G.B. analyzed and interpreted data; E.H., B.N., I.A.C., D.C.B., and G.B. performed statistical analysis; and E.H., B.J.M., S.J.F., and G.B. wrote the manuscript.

Conflict-of-interest disclosure: The authors declare no competing financial interests.

ORCID profiles: D.C.B., 0000-0001-8033-9810; S.J.F., 0000-0002-9142-2107; G.B., 0000-0002-7434-926X.

Correspondence: Gaetan Burgio, The John Curtin School of Medical Research, The Australian National University, 131 Garran Rd, Canberra, ACT 2601, Australia; e-mail: gaetan.burgio@anu.edu.au.

References

1. Kurata M, Suzuki M, Agar NS. Antioxidant systems and erythrocyte life-span in mammals. *Comp Biochem Physiol B.* 1993;106(3):477-487.
2. Lang E, Qadri SM, Lang F. Killing me softly - suicidal erythrocyte death. *Int J Biochem Cell Biol.* 2012;44(8):1236-1243.
3. Bosman GJ, Werre JM, Willekens FL, Novotný VM. Erythrocyte ageing in vivo and in vitro: structural aspects and implications for transfusion. *Transfus Med.* 2008;18(6):335-347.
4. Mock DM, Widness JA, Veng-Pedersen P, et al. Measurement of posttransfusion red cell survival with the biotin label. *Transfus Med Rev.* 2014; 28(3):114-125.
5. Tchernia G, Gauthier F, Mielot F, et al. Initial assessment of the beneficial effect of partial splenectomy in hereditary spherocytosis. *Blood.* 1993;81(8):2014-2020.
6. Lang F, Qadri SM. Mechanisms and significance of eryptosis, the suicidal death of erythrocytes. *Blood Purif.* 2012;33(1-3):125-130.
7. Kean LS, Brown LE, Nichols JW, Mohandas N, Archer DR, Hsu LL. Comparison of mechanisms of anemia in mice with sickle cell disease and beta-thalassemia: peripheral destruction, ineffective erythropoiesis, and phospholipid scramblase-mediated phosphatidylserine exposure. *Exp Hematol.* 2002;30(5):394-402.
8. Lang PA, Schenck M, Nicolay JP, et al. Liver cell death and anemia in Wilson disease involve acid sphingomyelinase and ceramide. *Nat Med.* 2007; 13(2):164-170.
9. Cappellini MD, Fiorelli G. Glucose-6-phosphate dehydrogenase deficiency. *Lancet.* 2008; 371(9606):64-74.
10. Lelliott PM, McMorran BJ, Foote SJ, Burgio G. The influence of host genetics on erythrocytes and malaria infection: is there therapeutic potential? *Malar J.* 2015;14:289.
11. Malaria Genomic Epidemiology Network. Reappraisal of known malaria resistance loci in a large multicenter study. *Nat Genet.* 2014;46(11): 1197-1204.
12. Koka S, Föller M, Lamprecht G, et al. Iron deficiency influences the course of malaria in Plasmodium berghei infected mice. *Biochem Biophys Res Commun.* 2007;357(3):608-614.
13. Foller M, Bobbala D, Koka S, Huber SM, Gulbins E, Lang F. Suicide for survival: death of infected erythrocytes as a host mechanism to survive malaria. *Cell Physiol Biochem.* 2009;24(3-4): 133-140.
14. Totino PR, Daniel-Ribeiro CT, Ferreira-da-Cruz MF. Refractoriness of eryptotic red blood cells to Plasmodium falciparum infection: a putative host defense mechanism limiting parasitaemia. *PLoS One.* 2011;6(10):e26575.
15. Bhavsar SK, Gu S, Bobbala D, Lang F. Janus kinase 3 is expressed in erythrocytes, phosphorylated upon energy depletion and involved in the regulation of suicidal erythrocyte death. *Cell Physiol Biochem.* 2011;27(5):547-556.
16. Hitomi Y, Cirulli ET, Fellay J, et al. Inosine triphosphate protects against ribavirin-induced adenosine triphosphate loss by adenylosuccinate synthase function. *Gastroenterology.* 2011; 140(4):1314-1321.
17. Sabina RL, Wandersee NJ, Hillery CA. Ca2+-CaM activation of AMP deaminase contributes to adenine nucleotide dysregulation and phosphatidylserine externalization in human sickle erythrocytes. *Br J Haematol.* 2009;144(3): 434-445.
18. Tavazzi B, Di Pierro D, Amorini AM, et al. Energy metabolism and lipid peroxidation of human erythrocytes as a function of increased oxidative stress. *Eur J Biochem.* 2000;267(3):684-689.
19. Mahnke DK, Sabina RL. Calcium activates erythrocyte AMP deaminase [isoform E (AMPD3)] through a protein-protein interaction between calmodulin and the N-terminal domain of the AMPD3 polypeptide. *Biochemistry.* 2005;44(14): 5551-5559.
20. Bauer DC, McMorran BJ, Foote SJ, Burgio G. Genome-wide analysis of chemically induced mutations in mouse in phenotype-driven screens. *BMC Genomics.* 2015;16(1):866.
21. Li H, Durbin R. Fast and accurate short read alignment with Burrows-Wheeler transform. *Bioinformatics.* 2009;25(14):1754-1760.
22. Langmead B, Salzberg SL. Fast gapped-read alignment with Bowtie 2. *Nat Methods.* 2012;9(4): 357-359.
23. Li H, Handsaker B, Wysoker A, et al; 1000 Genome Project Data Processing Subgroup. The Sequence Alignment/Map format and SAMtools. *Bioinformatics.* 2009;25(16):2078-2079.
24. McKenna A, Hanna M, Banks E, et al. The Genome Analysis Toolkit: a MapReduce framework for analyzing next-generation DNA sequencing data. *Genome Res.* 2010;20(9): 1297-1303.
25. Wang K, Li M, Hakonarson H. ANNOVAR: functional annotation of genetic variants from high-throughput sequencing data. *Nucleic Acids Res.* 2010;38(16):e164.
26. Laemmli U. Cleavage of structural proteins during the assembly of the head of bacteriophage T4. *Nature.* 1970;227:680-685.
27. Creek DJ, Jankevics A, Burgess KE, Breitling R, Barrett MP. IDEOM: an Excel interface for analysis of LC-MS-based metabolomics data. *Bioinformatics.* 2012;28(7):1048-1049.
28. Dunn WB, Erban A, Weber RJM, et al. Mass appeal: metabolite identification in mass spectrometry-focused untargeted metabolomics. *Metabolomics.* 2013;9(1):S44-S66.
29. Sumner LW, Amberg A, Barrett D, et al. Proposed minimum reporting standards for chemical analysis Chemical Analysis Working Group (CAWG) Metabolomics Standards Initiative (MSI). *Metabolomics.* 2007;3(3):211-221.
30. Chen K, Liu J, Heck S, Chasis JA, An X, Mohandas N. Resolving the distinct stages in erythroid differentiation based on dynamic changes in membrane protein expression during erythropoiesis. *Proc Natl Acad Sci USA.* 2009; 106(41):17413-17418.
31. Lelliott PM, Lampkin S, McMorran BJ, Foote SJ, Burgio G. A flow cytometric assay to quantify invasion of red blood cells by rodent Plasmodium parasites in vivo. *Malar J.* 2014;13:100.
32. Yap GS, Stevenson MM. Plasmodium chabaudi AS: erythropoietic responses during infection in resistant and susceptible mice. *Exp Parasitol.* 1992;75(3):340-352.
33. Min-Oo G, Fortin A, Tam MF, Nantel A, Stevenson MM, Gros P. Pyruvate kinase deficiency in mice protects against malaria. *Nat Genet.* 2003;35(4):357-362.
34. Chang KH, Stevenson MM. Malarial anaemia: mechanisms and implications of insufficient erythropoiesis during blood-stage malaria. *Int J Parasitol.* 2004;34(13-14):1501-1516.

35. Lowy B, Dorfman BZ. Adenylosuccinase activity in human and rabbit erythrocyte lysates. *J Biol Chem.* 1970;245(12):3043-3046.

36. Lowy BA, Williams MK, London IM. Enzymatic deficiencies of purine nucleotide synthesis in the human erythrocyte. *J Biol Chem.* 1962;237: 1622-1625.

37. Bader-Meunier B, Gauthier F, Archambaud F, et al. Long-term evaluation of the beneficial effect of subtotal splenectomy for management of hereditary spherocytosis. *Blood.* 2001;97(2): 399-403.

38. Lang E, Lang F. Mechanisms and pathophysiological significance of eryptosis, the suicidal erythrocyte death. *Semin Cell Dev Biol.* 2015;39:35-42.

39. Weiden PL, Robinett B, Graham TC, Adamson J, Storb R. Canine cyclic neutropenia. A stem cell defect. *J Clin Invest.* 1974;53(3):950-953.

40. Horwitz M, Benson KF, Person RE, Aprikyan AG, Dale DC. Mutations in ELA2, encoding neutrophil elastase, define a 21-day biological clock in cyclic haematopoiesis. *Nat Genet.* 1999; 23(4):433-436.

41. Lei J, Mackey MC. Understanding and treating cytopenia through mathematical modeling. *Adv Exp Med Biol.* 2014;844:279-302.

42. Dale DC, Person RE, Bolyard AA, et al. Mutations in the gene encoding neutrophil elastase in congenital and cyclic neutropenia. *Blood.* 2000; 96(7):2317-2322.

43. Grenda DS, Murakami M, Ghatak J, et al. Mutations of the ELA2 gene found in patients with severe congenital neutropenia induce the unfolded protein response and cellular apoptosis. *Blood.* 2007;110(13):4179-4187.

44. Cortes JE, Talpaz M, Kantarjian H. Chronic myelogenous leukemia: a review. *Am J Med.* 1996;100(5):555-570.

45. Mackey MC. Periodic auto-immune hemolytic anemia: an induced dynamical disease. *Bull Math Biol.* 1979;41(6):829-834.

46. Omodeo-Salè F, Motti A, Basilico N, Parapini S, Olliaro P, Taramelli D. Accelerated senescence of human erythrocytes cultured with Plasmodium falciparum. *Blood.* 2003; 102(2):705-711.